On the influence of a patterned substrate on crystallization in suspensions of hard spheres

Sven Dorosz and Tanja Schilling

Theory of Soft Condensed Matter, Université du

Luxembourg, L-1511 Luxembourg, Luxembourg

Abstract

We present a computer simulation study on crystal nucleation and growth in supersaturated suspensions of mono-disperse hard spheres induced by a triangular lattice substrate. The main result is that compressed substrates are wet by the crystalline phase (the crystalline phase directly appears without any induction time), while for stretched substrates we observe heterogeneous nucleation. The shapes of the nucleated crystallites fluctuate strongly. In the case of homogeneous nucleation amorphous precursors have been observed (Phys. Rev. Lett. 105(2):025701 (2010)). For heterogeneous nucleation we do not find such precursors. The fluid is directly transformed into highly ordered crystallites.

PACS numbers: 82.60.Nh, 64.60.Q-, 64.60.qe, 64.70.pv, 68.55.A-

When a supersaturated fluid crystallizes, crystallization is usually induced by the container walls, rather than to proceed from a fluctuation in the bulk of the system. This effect, called heterogeneous nucleation, is of fundamental importance for the kinetics of phase transitions (such as the formation of ice in the supersaturated vapor of clouds), as well as for technological applications, in which the properties of the walls can be designed to influence the properties of the crystals that are formed. In this article we discuss heterogeneous crystal nucleation and growth from the overcompressed fluid of hard spheres.

Hard spheres have served successfully as a simple model system for fluids and crystals over the past fifty years. The interaction energy between two hard spheres is either infinite (if they overlap) or zero (if they do not overlap), thus the phase behavior of the model is purely determined by entropy. The simplicity of the potential makes hard spheres particularly suited for computer simulations; and the entropic nature of the phase transition makes them a useful limit case for comparison to other systems, which are governed by an interplay between entropy and enthalpy.

Hard spheres are not only of interest to the theoretician, they are also often synthesized on the colloidal scale and used in experiments on fundamental questions of statistical mechanics (see e. g. [1] and references therein).

As the topic of our work, crystallization of hard spheres on a substrate, has been studied experimentally [2–7] and theoretically [8–16] before, we briefly lay out in the following, which aspects of this topic have been focused on in the articles cited above.

The supersaturated fluid of hard spheres in contact with a planar hard wall has been addressed in computer simulation studies by Dijkstra [9], Auer [8] and Volkov [10]. These studies show that the planar hard wall is wet by the crystalline phase, hence crystallization proceeds layer by layer rather than by the nucleation of crystallites. (For a review on wetting and film growth of crystalline phases on structured and unstructured surfaces in various systems, including hard spheres, see the article by Esztermann and Löwen [15].) Also the recent experimental and simulation work by Sandomirski and co-workers [7] dealt with the growth of a crystalline film in contact with a wall. Here the wall was not planar but a

fcc layer of spheres. The authors found that the speed of the crystallization front depends non-monotonically on the packing fraction of the fluid and that a depletion zone is present in front of the growing crystal.

Heterogeneous nucleation of hard sphere crystals has mainly been addressed in the context of template-induced crystallization. Van Blaaderen and co-workers [3–5] showed how to design structured templates to induce the epitaxial growth of large monocrystals and of metastable phases in a sedimenting liquid of hard spheres. Cacciuto and Frenkel studied the effect of finite templates of various sizes and lattice structures on crystallite formation by means of computer simulation [12]. Recently this topic was taken up again and investigated in more detail experimentally and theoretically by the groups of Dijkstra and van Blaaderen [6]. For small two-dimensional seeds of triangular as well as square symmetry they find that nucleation barriers depend on the seed's symmetry as well as the lattice spacing. This effect is due to defects and changes in crystal morphology that are induced by the seed.

Heterogeneous nucleation of hard spheres on an infinite substrate has recently been addressed by Xu and co-workers [11] in a computer simulation study. In this work triangular and square substrates as well as a hcp(1100) pattern were brought in contact with a strongly overcompressed fluid, and the evolution of the density profile perpendicular to the substrate as well as the fraction of crystalline particles were monitored. A metastable bcc-phase that was stabilized for long times was observed.

Here we present an extended simulation study of crystallization mechanisms and rates for a fluid of hard spheres brought in contact with a triangular substrate for varying overcompression and lattice distortion. To our knowledge there is no systematic study on the effect that distortion of an infinite substrate lattice has on the crystallization mechanism and rate of hard spheres.

We would like to close this brief overview by pointing out that there are other useful model systems for crystal nucleation, as e. g. complex plasmas. In contrast to colloidal systems microscopic dynamics in complex plasmas are almost undamped, [17] hence they offer a complementary experimental approach to the topic.

I. SETUP OF THE SYSTEM AND SIMULATION DETAILS

The simulations were carried out by means of an event driven molecular dynamics program for fixed particle number, volume and energy (for details on event driven MD see refs. [18–21]). We simulated N=216,000 hard spheres of diameter σ in contact with a substrate of triangular symmetry formed by N=4200 spheres of the same diameter σ . The substrate particles were immobile (i.e. they had infinite mass). The simulation box had periodic boundaries in x and y directions. The substrate layers were fixed at $z=\pm \frac{L_z}{2}$ for $L_z=30\sigma\ldots50\sigma$, depending on the overcompression. The initial velocities were drawn from a Gaussian distribution and the initial mean kinetic energy per particle was set to $3 k_B T$.

To monitor crystallinity, we used the local q6q6-bond-order parameter [22, 23], which is defined as follows: For each particle i with n(i) neighbors, the local bond-orientational structure is characterized by

$$\bar{q}_{6m}(i) := \frac{1}{n(i)} \sum_{j=1}^{n(i)} Y_{6m}(\vec{r}_{ij})$$
 ,

where $Y_{6m}(\vec{r}_{ij})$ are the spherical harmonics with l=6. \vec{r}_{ij} is the displacement between particle i and its neighbor j in a given coordinate frame. A vector $\vec{q}_6(i)$ is assigned to each particle, the elements $m=-6\ldots 6$ of which are defined as

$$q_{6m}(i) := \frac{\bar{q}_{6m}(i)}{\left(\sum_{m=-6}^{6} |\bar{q}_{6m}(i)|\right)^{1/2}} . \tag{1}$$

We counted particles as neighbors if their distance satisfied $|\vec{r}_{ij}| < 1.4\sigma$. Two neighboring particles i and j were regarded as "bonded" within a crystalline region if $\vec{q}_6(i) \cdot \vec{q}_6(j) > 0.7$. We define $n_b(i)$ as the number of "bonded" neighbors of the ith particle. (In the online version we use the following colour-coding for the snapshots: if a particle has $n_b > 10$, i.e. an almost perfectly hexagonally ordered surrounding, it is color-coded green, if $n_b > 5$ it is color-coded brown.)

We studied various densities between particle number density $\rho := N\sigma^3/V = 1.005$ (which corresponds to a volume fraction $\eta = 0.5262$) and $\rho = N\sigma^3/V = 1.02$ ($\eta = 0.5341$). At

these densities the chemical potential difference per particle between the metastable fluid and the stable crystalline state is between $\Delta\mu \simeq -0.5~k_BT$ and $\Delta\mu \simeq -0.54~k_BT$. The overcompressed fluid configurations did not show pre-existing crystallites that might have been created during the preparation process.

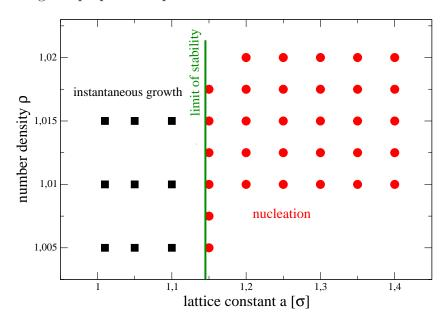


FIG. 1: Representation of all combinations of density ρ and substrate lattice constant a studied in this work. The limit of stability of the homogeneous bulk crystal is indicated by the solid line (green online). At substrate lattice constants smaller than this value (squares) we find complete wetting of the substrate and instantaneous film growth. Systems with a larger substrate lattice constant (circles) exhibit incomplete wetting and heterogeneous nucleation up to $a \leq 1.5\sigma$. Above this stretching, no heterogeneous nucleation event was observed on the scale of the simulation time.

Figure 1 shows the densities ρ and substrate lattice constants a (of the fcc-(111) plane) for which we carried out simulations. The lattice constant indicated by the solid line (green online) corresponds to the bulk crystal at the spinodal, i.e. at the density at which the crystal ceases to be metastable with respect to the liquid. We obtained this density by simulation as well as from density functional theory [24]. The corresponding lattice constant is $a_{\rm sp} = 1.15\sigma$ (DFT) resp. $a_{\rm sp} = 1.14\sigma$ (simulation). One result of our study is that this

line separates the parameter space into regions of different crystallization mechanisms. For $a < a_{\rm sp}$, we observed the instantaneous formation of a film, which then grew with time. For $a > a_{\rm sp}$, the system crystallized via heterogeneous nucleation. The transition between the two mechanisms seems to be continuous. For $a \ge 1.5\sigma$ no heterogeneous nucleation event was observed on the scale of the simulation time.

II. COMPLETE WETTING OF THE SUBSTRATE

For all compressed substrates ($a < a_{\rm sp}$) we observed the formation and growth of a crystalline film. Typical snapshots are presented in figure 2. (Here, we chose a system at $a = 1.1\sigma$, close to $a_{\rm sp}$, and a bulk density of $\rho = 1.01$.) The timescale of the MD simulation is expressed in multiples of $\tau = \frac{\sigma^2}{6D}$, with D being the long-time self diffusion coefficient in the bulk fluid obtained in the same MD simulations. In the regime of densities analyzed, the diffusion constant varies by only 5%.)

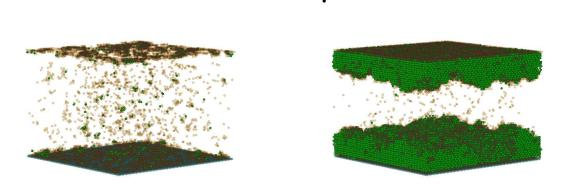


FIG. 2: Snapshots $t = \tau$ (left) and $t = 100\tau$ after bringing the overcompressed fluid in contact with the substrate, $a = 1.1\sigma$ (slightly less than $a_{\rm sp}$), $\rho = 1.01$. Only crystalline particles are shown $(n_b > 5)$

In order to analyze the crystalline layers quantitatively, we computed the 2-dimensional

bond-order parameter ψ_6 for planes perpendicular to the z-direction. (ψ_6 is the 2d equivalent of \bar{q}_6 .)

$$\psi_6(i) := \frac{1}{n(i)} \sum_{i=1}^{n(i)} e^{i6\theta_{ij}} ,$$

where θ_{ij} is the angle of the vector \vec{r}_{ij} and an arbitrary but fixed axis in the plane. We impose a cut-off at $|\vec{r}_{ij}| < 1.4\sigma$ and demand for a crystalline particle that $\psi_6(i)\psi_6^*(j) > 0.7$ for six neighbors.

To discuss the analysis in detail, we pick three substrate lattice constants $a = \{1.01\sigma, 1.05\sigma, 1.1\sigma\}$ at a fixed density $\rho = 1.005$.

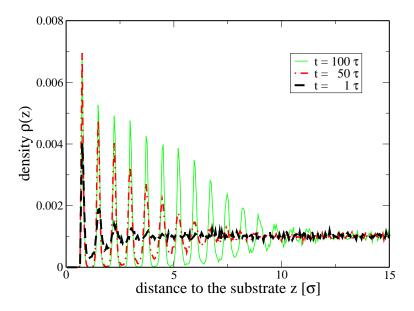


FIG. 3: Density profile perpendicular to the substrate for half of the system at different times. $\rho = 1.01$, $a = 1.1\sigma$. A film of layers grows.

Figure 3 shows a vertical density profile. As a function of time the layering becomes more pronounced, as seen from the growth of the maxima and the appearance of voids in between the layers. (A quantitative analysis of the growth rate for different substrate lattice constants is not reported, because the lateral dimension was too small.) According to these profiles we identify the particles that belong to a given layer and study the hexagonal structure in the

plane. The overall defect density η in a given layer n with a total numer of N(n) particles is defined as

$$\eta(n) := \frac{N(n) - N_{\text{crys}(n)}}{N(n)},\tag{2}$$

with $N_{\text{crys}}(n)$ being the number of crystalline particles in layer n. The analysis of the defect density is shown in figure 4. We have also included the total number of particles N(n) in each layer n for the three cases of a. The further the substrate is compressed with respect to the equilibrium lattice the larger is the defect density in the first layer. With larger distance from the substrate the defect density for all three values of a converges to a substrate independent value. At this point stresses induced by the substrate do not play a role in the growing crystal anymore. Only the tension induced by the shape of the periodic box, which is not commensurate with the equilibrium lattice, matters.

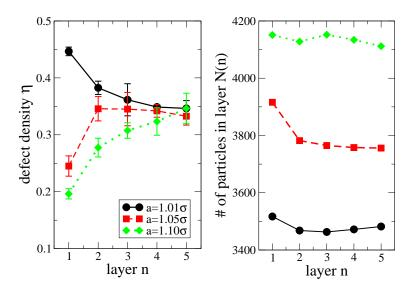


FIG. 4: (left) Defect density as a function of the index of each layer counted from the substrate for three different substrate lattice constants. The data shown has been obtained in the long time limit $t > 400 \tau$ and it is averaged over three independent runs each.

(right) Number of particles N(n) in each layer n.

Figure 5 shows the covering of the substrate for the first three layers after $t = 400 \tau$. There is no preference of fcc over hcp. An analysis of the subsequent layers showed that the stacking is

random-hcp. This is in agreement with the small free energy difference of $26\pm6\cdot10^{-5}k_BT/\sigma^2$ per particle [25]. Domains of equal structure are much larger for the case $a=1.1\sigma$ than for $a=1.01\sigma$, where there are more domain walls. No single crystal phase evolved on the recorded timescales.

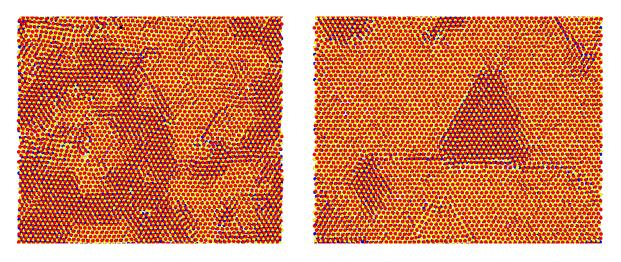


FIG. 5: Snapshot of the first three layers on top of the substrate for (left) $a = 1.01\sigma$ and (right) $a = 1.10\sigma$. The snapshots correspond to the data analyzed in figure 4. There is no preference of fcc over hcp.

III. HETEROGENOUS NUCLEATION NEAR THE SUBSTRATE

For the parameter regime $1.15\sigma \le a \le 1.4\sigma$ we observe the formation of crystallites at the substrate. Figure 6 shows snapshots of typical crystallites at the first nucleation event (figure 6a) and at a much later time (figure 6b).

We define the nucleation event as the moment when the first crystalline cluster reaches a size of 100 particles, see figure 6a for a snapshot. In all simulations we observed irreversible growth above this threshold. Below this threshold crystallites appeared and decayed again. Changing this value by ± 10 particles does not affect any of the results presented in the



FIG. 6: Snapshots at different times after bringing the overcompressed fluid in contact with the substrate, $a=1.4\sigma$, $\rho=1.01$. Crystallite formation at the wall dominates the nucleation process. For clarity, we are not showing the substrate. Figure (a) shows the nucleation event at which the first crystallite reaches 100 solid particles. Figure (b) shows the state of the system at a much later time.

following.

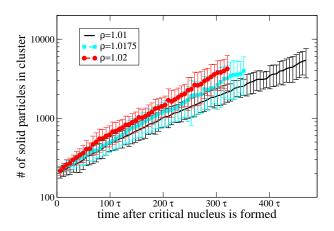


FIG. 7: Time evolution of size of the largest cluster for varying density ρ . The data is averaged over 8 independent runs at each given density.

In figure 7, we show that the mean size of the largest crystallite can be described by a growth law that is approximately exponential with time once the nucleation event has set in. (The timescale is reset to the nucleation event for each simulation run to compare the growth law. For each pair of a and ρ all data shown here is averaged over 8 independent runs.)

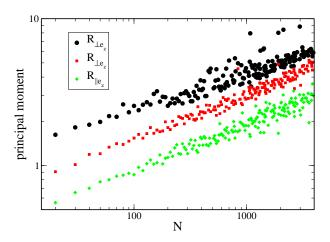


FIG. 8: Eigenvalues of the gyration tensor for all crystallites observed during the simulation at $a = 1.4\sigma$ and $\rho = 1.01$. The data is plotted independent of time as a function of the number of solid particles in the crystallite. It was checked that the eigenvector of the smallest eigenvalue is perpendicular to the substrate surface.

The structure of the nuclei is analyzed by means of the tensor of gyration, which we diagonalized to obtain the principal moments. We identified the eigenvector with the smallest eigenvalue $\vec{e}_{\rm small}$ and checked that it was parallel to the substrate normal ($\vec{e}_{\rm small} \cdot \vec{e}_z > 0.9$ is satisfied by more than 90% of the crystallites, however deviations are stronger for small crystallites of less than 50 particles). As a function of the total number of particles in a crystallite we present the principal moments in figure 8. Even up to $N_{\rm crys} = 4000$ the statistics do not support the interpretation of the droplets growing as a spherical cap (or any other simple geometry) on the substrate. They are rather ramified instead.

In the case of homogeneous nucleation from the overcompressed bulk fluid in hard spheres, a process mediated by amorphous precursors has been observed [26, 27]. We carefully checked the heterogeneous nucleation data and did not find any evidence of such precursors of low

crystalline symmetry. Nucleation at the substrate immediately produces highly ordered crystallites. Presumably the orientational symmetry breaking due to the substrate suffices to significantly reduce the induction time needed to create bond-orientational order.

TABLE I: Nucleation rates for different substrate lattice spacings a and densities ρ . All rates averaged over 8 runs. The rates are given in units of $6D/\sigma^5$.

$\rho \setminus a$	1.15σ	1.20σ	1.25σ	1.30σ	1.35σ	1.40σ
1.005	$1.3 \pm 0.2 \cdot 10^{-5}$					
1.0075	$1.4 \pm 0.2 \cdot 10^{-5}$					
1.01	$1.4 \pm 0.2 \cdot 10^{-5}$	$1.1 \pm 0.2 \cdot 10^{-5}$	$7.5 \pm 0.7 \cdot 10^{-6}$	$4.8 \pm 0.5 \cdot 10^{-6}$	$3.7 \pm 0.5 \cdot 10^{-6}$	$2.0 \pm 0.4 \cdot 10^{-6}$
1.0125	$1.5 \pm 0.2 \cdot 10^{-5}$	$1.1 \pm 0.1 \cdot 10^{-5}$	$7.9 \pm 0.8 \cdot 10^{-6}$	$5.2 \pm 0.6 \cdot 10^{-6}$	$4.0 \pm 0.6 \cdot 10^{-6}$	$2.1 \pm 0.5 \cdot 10^{-6}$
1.015	$1.5 \pm 0.2 \cdot 10^{-5}$	$1.2 \pm 0.1 \cdot 10^{-5}$	$8.5 \pm 0.7 \cdot 10^{-6}$	$5.6 \pm 0.6 \cdot 10^{-6}$	$4.8 \pm 0.8 \cdot 10^{-6}$	$2.3 \pm 0.4 \cdot 10^{-6}$
1.0175	$1.6 \pm 0.2 \cdot 10^{-5}$	$1.3 \pm 0.1 \cdot 10^{-5}$	$8.8 \pm 0.9 \cdot 10^{-6}$	$6.0 \pm 0.8 \cdot 10^{-6}$	$4 \pm 1 \cdot 10^{-6}$	$2.8 \pm 0.5 \cdot 10^{-6}$
1.02		$1.3 \pm 0.1 \cdot 10^{-5}$	$9\pm1\cdot10^{-6}$	$5.9 \pm 0.7 \cdot 10^{-6}$	$4.6 \pm 0.8 \cdot 10^{-6}$	$2.8 \pm 0.4 \cdot 10^{-6}$

Figure 9(left) shows the nucleation rates as a function of the substrate lattice constant for different bulk densities (also listed in table I.) We determine the nucleation rate by averaging over the times required to form the first cluster for 8 independent trajectories. (We did not include the times for subsequent events. Hence, the nucleation rates should not be affected by interactions between clusters, as they occur close to the line of stability.) Compared to the bulk nucleation rates, (see e. g. ref. [26, 28] for a compilation of experimental as well as simulation results), we note that the heterogeneous nucleation rates are increased by several orders of magnitude especially at low densities. It is remarkable that the nucleation rates do not decrease exponentially as in the homogeneous case for smaller densities. We rather observe, in figure 9(right) a linear decrease in this regime of densities. This linear behavior is seen for all lattice constants that we analyzed. The slopes do not show a significant dependence on a.

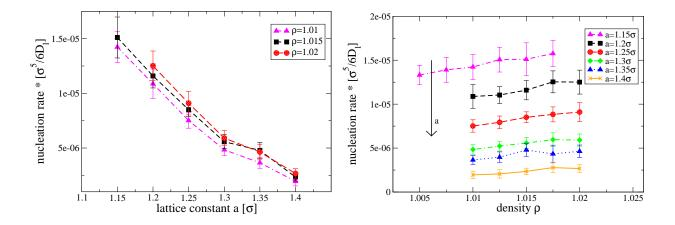


FIG. 9: (left) Nucleation rates as a function of the substrate lattice constant a in the regime of droplet formation for different bulk densities ρ . The nucleation rates are expressed in units of $\frac{\sigma^5}{6D}$. (right) Nucleation rates as a function of the bulk density ρ for different substrate lattice constants a.

A. Conclusion

We have studied the crystallization of an overcompressed fluid of hard spheres in contact with a fixed triangular lattice substrate by means of event driven molecular dynamics simulation. Depending on the lattice constant of the substrate, the system either crystallizes directly, without an induction time, or it crystallizes via nucleation. The value of the lattice constant that separates the two regimes is the value at which the bulk crystal, when being stretched, becomes unstable with respect to the liquid. If the substrate lattice constant is smaller than this value crystallization proceeds via the formation of a complete film which grows layer by layer. The stacking is random-hcp with a large density of defects.

If the substrate is stretched to lattice constants at which the bulk crystal is unstable, crystallization proceeds via heterogeneous nucleation. For moderate stretching, the nucleation rates are larger by several orders of magnitude with respect to homogeneous nucleation. The crystallites that are formed are very irregular in shape even when they contain up to several thousand particles.

In the case of homogeneous nucleation amorphous precursors have been observed [26, 27]. For heterogeneous nucleation we do not find such precursors. The fluid is directly transformed into highly ordered crystallites.

Acknowledgments

We thank Hamed Maleki, Koos van Meel, Martin Oettel, and Friederike Schmid. This project has been financially supported by the DFG (SFB Tr6 and SPP1296) and by the National Research Fund, Luxembourg co-funded under the Marie Curie Actions of the European Commission (FP7-COFUND). Computer simulations presented in this paper were carried out using the HPC facility of the University of Luxembourg.

- [1] W. C. K. Poon, E. R. Weeks, and C. P. Royall arXiv:1106.2566v1, 2011.
- [2] J. P. Hoogenboom, P. Vergeer, and A. van Blaaderen, The Journal of Chemical Physics, 119(6):3371-3383, 2003.
- [3] J. P. Hoogenboom, A. K. van Langen-Suurling, J. Romijn, and A. van Blaaderen, Phys. Rev. Lett., 90(13), 138301-+, 2003.
- [4] J. P. Hoogenboom, A. K. van Langen-Suurling, J. Romijn, and A. van Blaaderen, Phys. Rev. E, 69(5):051602, 2004.
- [5] A. van Blaaderen, R. Ruel, and P. Wiltzius, Nature, 385:321-324, 1997.
- [6] M. Hermes, E. C. M. Vermolen, M. E. Leunissen, D. L. J. Vossen, P. D. J. van Oostrum, M. Dijkstra, A. van Blaaderen, Soft Matter, 7, 10, 2011.
- [7] K. Sandomirski, E. Allahyarov, H. Löwen, and S. U. Egelhaaf, Soft Matter, 7, 18, 2011.
- [8] S. Auer and D. Frenkel, Phys. Rev. Lett., 91(1):015703, 2003.
- [9] M. Dijkstra, Phys. Rev. Lett., 93(10):108303, 2004.
- [10] I. Volkov, M. Cieplak, J. Koplik, and J. R. Banavar, Phys. Rev. E, 66(6):061401, 2002.
- [11] W.-S. Xu, Z.-Y. Sun, and L.-J. An., Journal of Chemical Physics, 132(14):144506, 2010.

- [12] A. Cacciuto and D. Frenkel, Phys. Rev. E, 72(4):041604, 2005.
- [13] M. Heni and H. Löwen, Journal of Physics: Condensed Matter, 13:4675-4696, 2001.
- [14] M. Heni and H. Löwen, Phys. Rev. Lett, 85:3668-3671, 2000.
- [15] A. Esztermann and H. Löwen, Journal of Physics: Condensed Matter, 17(9):S429, 2005.
- [16] H. Wang, H. Gould, and W. Klein, Phys. Rev. E, 76, 031604, 2007.
- [17] M. Rubin-Zuzic, G. E. Morfill, A. Ivlev, R. Pompl, B. A. Klumov, W. Bunk, H. M. Thomas, H. Rothermel, O. Havnes, and A. Fouquet, Nature Physics 2, 181, 2006.
- [18] B. J. Alder and T. E. Wainwright, The Journal of Chemical Physics, 31(2):459-466, 1959.
- [19] A. T. Krantz, ACM Trans. Model. Comput. Simul., 6:185209, 1996.
- [20] B. D. Lubachevsky, J. Comput. Phys., 94:255-283, 1991.
- [21] M. Marin and P. Cordero, Computer Physics Communications, 92(2-3):214-224, 1995.
- [22] P. J. Steinhardt, D. R. Nelson, and M. Ronchetti, Phys. Rev. B, 28(2):784-805, 1983.
- [23] P. R. ten Wolde, M. J. Ruiz-Montero, and D. Frenkel, Phys. Rev. Lett., 75(14):2714-2717, 1995.
- [24] M. Oettel, private communication.
- [25] S. Pronk and D. Frenkel, Journal of Chemical Physics, 110(9), 4589-4592, 1999.
- [26] T. Schilling, S. Dorosz, H. J. Schöpe, and G. Opletal, Journal of Physics: Condensed Matter, 23(19):194120, 2011.
- [27] T. Schilling, H. J. Schöpe, M. Oettel, G. Opletal, and I. Snook, Phys. Rev. Lett., 105(2):025701, 2010.
- [28] L. Filion, M. Hermes, R. Ni and M. Dijkstra, The Journal of Chemical Physics, 133(24), 244115, 2010.